Supporting Information

Foffi et al. 10.1073/pnas.1406990111

SI Text

Appendix: Further Details of SAXS Intensities and Structure Factor Modeling, Viscosity at Low- and High-Volume Fractions, MD Results, and Methods. Fig. S1 shows the measured SAXS intensities $I(q)$ vs. scattering vector magnitude q, as a function of α-crystallin weight per volume concentration, c. $I(q)$ at $c_0 = 5$ mg/mL was used to derive the measured form factor $P_M(q)$. $P_M(q)$ was then used to determine the $S_M(q)$, as described in Figs. 1 and 3 in the main text.

For the polydisperse hard-sphere liquid-structure model (PHSM) used (1), we take the distribution of particle diameters d to have number-average diameter $\overline{d}$ and normalized, dimensionless SD $\sigma^2 = (\overline{d^2}/\overline{(d)}^2) - 1$ and model it as a Schulz (or generalized exponential) distribution with probability density function $f(d)$, where

$$f(d) = \frac{y^z e^{-y/\sigma^2}}{\overline{d}\,\Gamma(z+1)(\sigma^2)^{z+1}} \qquad \text{[S1]}$$

in which $z = (1/\sigma^2) - 1$ and $y = d/\overline{d}$. Here $\sigma = p$, the polydispersity index used in the text.

Vrij (1) derived the Percus–Yevick $S_{M,\mathrm{PY}}(0)$ in terms of the first six moments $\mathcal{M}_\nu$ of any particle diameter distribution,

$$S_{M,\mathrm{PY}}(0) = \frac{(1-\phi)^4}{(1+2\phi)^2}\left[1 + \frac{6\phi(1+2\phi)}{(1-\phi)^2}\times\left(1 - \frac{\mathcal{M}_4\mathcal{M}_5}{\mathcal{M}_3\mathcal{M}_6}\right) - \frac{9\phi^2}{(1-\phi)^2}\times\left(1 - \frac{\mathcal{M}_4^3}{\mathcal{M}_3^2\mathcal{M}_6}\right)\right] \qquad \text{[S2]}$$

in which $\mathcal{M}_\nu = \overline{d^\nu}/\overline{d}^\nu$ and the volume fraction $\phi = (\pi/6V)\sum_{i=1}^{N}\rho_i d_i^3$, and d_i is the diameter of particle i. The moments of the Schulz distribution are given by

$$\mathcal{M}_\nu = \left[1 + (\nu-1)\sigma^2\right]\left[1 + (\nu-2)\sigma^2\right]\cdots\left[1 + \sigma^2\right]1. \qquad \text{[S3]}$$

Using Eq. **S3** in Eq. **S2**, one obtains

$$S_{M,\mathrm{PY}}(0) = \frac{(1-\phi)^4}{(1+2\phi)^2}\left[1 + \frac{6\phi(1+2\phi)}{(1-\phi)^2}\times A - \frac{9\phi^2}{(1-\phi)^2}\times B\right], \qquad \text{[S4]}$$

with which we fit the SAXS $S_M(q)$ data (Figs. 2 and 3 in main text):

$$A = \frac{(1+3\sigma^2)}{(1+5\sigma^2)};$$

$$B = \frac{(1+3\sigma^2)^2}{(1+5\sigma^2)(1+4\sigma^2)}.$$

To study how well $S_{M,\mathrm{PY}}(q)$ fits the data as a function of p and $\overline{d}$ (Fig. 3, *Bottom*), we used R^2 defined as

$$R^2 = 1 - \frac{SS_{\mathrm{err}}}{SS_{\mathrm{tot}}},$$

where the sum of square residuals $\mathrm{SS_{err}}$ and the total sum of squares $\mathrm{SS_{tot}}$ are given by

$$\mathrm{SS_{err}} = \sum_{i=1}^{n^*}\left[S_M(q_i) - S_{M,\mathrm{PY}}(q_i)\right]^2$$

$$\mathrm{SS_{tot}} = \sum_{i=1}^{n^*}\left[S_M(q_i) - \overline{S_M}\right]^2. \qquad \text{[S5]}$$

We note that for a fit to a linear model, the coefficient of determination R^2 varies between 0 and 1, being closer to 1 when the fit perfectly reproduces the data. In the present nonlinear context, R^2 can take negative values when simple averages reproduce the data better than the proposed model. Here we use R^2 only as a means to estimate the sensitivity of $S_{M,\mathrm{PY}}(q)$ fits to p and $\overline{d}$. We limited the sums in Eq. **S5** to the first peak of $S_M(q)$, by taking the first $n*$ points such that $q_{n*} \le 0.8$ nm^{-1}; $\overline{S_M}$ is the average of the experimental values of $S_M(q)$ for the first $n*$ points. Fig. S2 shows $1 - R^2$ goodness-of-fit values (colors and contours) as a function of the assumed polydispersity parameter, p, and α-crystallin number-average diameter, $\overline{d}$. The plots show that $p = 0.20$ and $d = 15$ nm (white crosses) are quite close to parameter-space minima of $1 - R^2$ for Percus–Yevick fits of $S_M(q)$, for α-crystallin concentrations shown in Fig. 3 of the text.

Fig. S3 shows the relative viscosity η_r at low and high α-crystallin volume fractions ϕ, amplifying these ranges for the data shown in Fig. 2 (*Top*) of the main text. The low-concentration data yield intrinsic viscosity $[\eta] = 5.5 \pm 0.5$, in agreement with full Krieger–Dougherty fit. The high-concentration power-law dependence (Fig. 2, *Bottom*) of η_r on $|\phi_c - \phi|$, following mode-coupling theory, gives $\gamma = 2.8$ with $\phi_c = 0.58 \pm 0.02$. For the Krieger–Dougherty functional form, $\phi_m = 0.579 \pm 0.004$. Thus, $\phi_c = \phi_m$ within the uncertainty in the fits. The exponent α is equal to $1/([\eta]\phi_m)$ and $1/\gamma$ for the KD and MCT fits, respectively.

Fig. S4 shows mean-square displacements (MSD) vs. time and ISFs from simulations at volume fractions approaching the ϕ_c expected for monodisperse HS systems. Fig. S4 shows the results for $q = 0.0366$ nm^{-1}, the smallest q attempted due to long computational times required for larger simulation boxes. Note that the minimum q for MD is comparable to but larger than $q = 0.023$ nm^{-1} used for DLS. The initial rise and then flattening of the MSD with delay time shown in Fig. S4 (*Top*) is consistent with increased trapping of particles in cages of neighbors, as the concentration increases. The MD-simulated ISF in Fig. S4 (*Bottom*) shows features similar to those of the α-crystallin DLS data in Fig. 2 (*Bottom*) of main text. It is important to note that, unlike the idealized schematic in Fig. 4 (*Top*, *Inset*) of main text, a flat plateau in the MD-simulated ISF did not appear at high concentrations at this scattering vector, as is also the case for experimental α-crystallin ISFs obtained using DLS (Fig. 2, *Bottom*).

Fig. S5 shows an MD-simulated ISF and corresponding rectification plot at the volume fraction $\phi = 0.5925$, very near the volume fraction $\phi = 0.58$ for the experimental DLS ISF just below the glass transition, for which the analogous plots appear as in Fig. 4 in the main text. By the power-law fits, we obtain the MCT exponents $a = 0.31$ and $b = 0.49$, which correspond to $\gamma = 2.6$. These values are compatible with the experimental results.

Fig. S6 (*Top*) shows the number-average self-diffusion coefficients $D_{s,\mathrm{na}}$ derived from Fig. S4 (*Top*) vs. volume fractions ϕ, near ϕ_c. In Fig. S6, *Bottom*, replotting of the same data in the form $D^{1/\gamma}$ vs. $\phi_c - \phi$ shows power-law dependence for $\phi_c = 0.6074$ and $\gamma = 2.8$.

Further Details of Methods.

Sample preparation. Briefly, 4-mo-old calf eyes were obtained fresh from a local slaughterhouse and stored and handled at 4 °C. Lens capsules were removed and lens cortex was separated from nucleus. Cortical regions were homogenized 1:1 in phosphate buffer ($pH^{20°C}$ 7.0, ionic strength $I = 320$ mM, containing 34 mM NaH_2PO_4, 18 mM Na_2HPO_4, 200 mM NaCl,1 mM EDTA, 3 mM NaN_3, 3 mM DTT) and the suspension was centrifuged for 40 min at 18,500 × g at 4 °C to remove insoluble material. Size-exclusion chromatography was performed on diluted supernatant, using an Amersham Biosciences ÄKTA prime system and a Superdex S-200 PG column (Φ = 26 × 60cm; Amersham Biosciences) equilibrated with the same phosphate buffer, to separate α-crystallin from β- and γ-crystallins. Fractions from different preparations were collected and stored at 4 °C until enough material was obtained. This 3-mg/mL stock solution was concentrated to 100 mg/mL, using an Amicon ultrafiltration cell with a YM10 membrane (regenerated cellulose, nominal molecular weight limit:10,000), and then concentrated to more than 400 mg/mL in ultrafiltration cells, at 4,000 × g for 48 h. α-Crystallin concentration was determined spectrophotometrically after controlled dilution, using an absorption coefficient of $8.45^{1\%,\ 280\ nm}_{1\ cm}$.

Light scattering. Measurements were carried out at scattering angles between 40° and 130° with an angular step of 10°. Diffusivities D were determined from the initial decay of the normalized field autocorrelation functions through a second-order cumulant analysis. To get a good estimate for the plateau height of the nonergodic glass-like sample we measured the sample again while slowly rotating it at a rotation speed of 0.01 rpm, using the sample goniometer of the instrument, which introduces a forced decay and ensures proper ergodic averaging of the correlation function.

Simulation. Particle masses were chosen so that their density remained constant. Several runs at different packing fractions from independent initial conditions were performed to gain statistical accuracy on the MCT fits. Each simulation was sufficiently long to guarantee average overall displacements of at least five times the particle diameter or more than 1,000 "cage breaks" on average. The number-average long-time diffusion coefficient $D_{s,\mathrm{na}}$ was extracted from the MSD, using $\langle x^2 \rangle = 6D_{s,\mathrm{na}}t$ for each ϕ. Simulated intermediate scattering functions $f_M(q,t)$ were calculated vs. ϕ and q, averaging over up to 300 independent directions of $\mathbf{q}$.

1. Vrij A (1979) Mixtures of hard spheres in the Percus-Yevick approximation. Light scattering at finite angles. *J Chem Phys* 71:3267–3270.

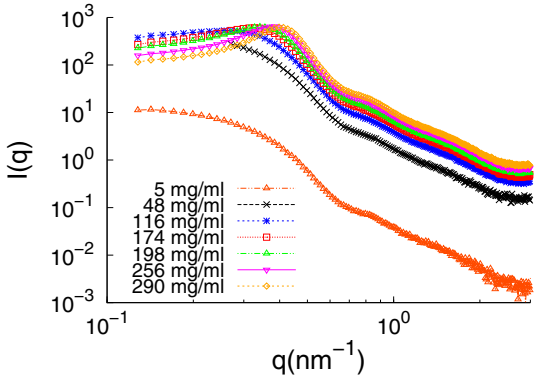

Fig. S1. SAXS $I(q)$ (scale arbitrary) vs. q as a function of α-crystallin concentration.

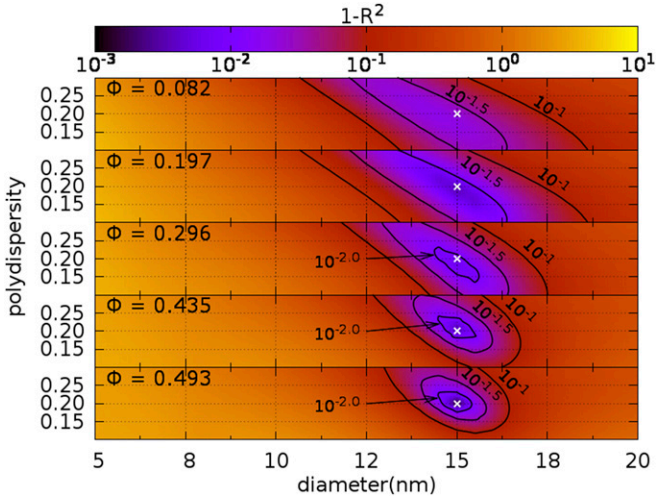

Fig. S2. The $1 - R^2$ goodness-of-fit values (colors and contours) as a function of the assumed polydispersity parameter, p, and α-crystallin number-average diameter, d (*SI Text* and Fig. 3 in main text). The concentrations are 48 mg/mL, 115 mg/mL, 174 mg/mL, 255 mg/mL, and 290 mg/mL from top to bottom.

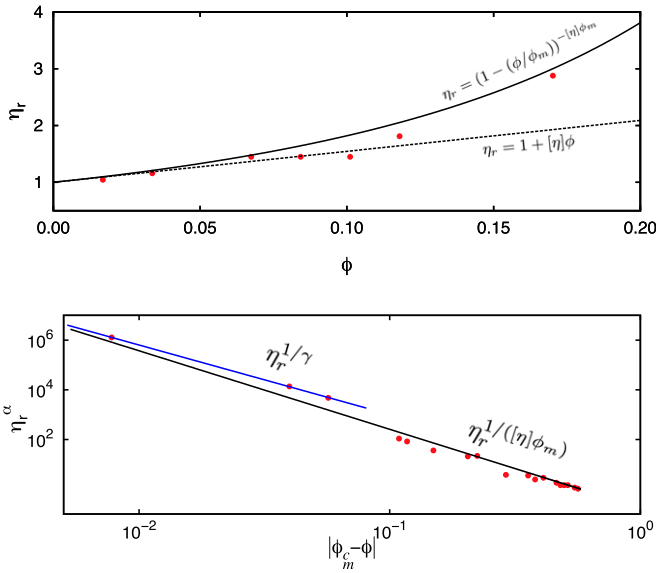

Fig. S3. Relative viscosity η_r at low (*Top*) and high (*Bottom*) α-crystallin volume fractions ϕ, amplifying these ranges for the data shown in Fig. 2 (*Top*) of the main text. Low-concentration data yield intrinsic viscosity $[\eta] = 5.5$, in agreement with full Krieger–Dougherty fit. High-concentration power-law dependence of η_r on $|\phi_c - \phi|$ gives $\gamma = 2.8$; $\phi_c = 0.579$. The exponent α is equal to $1/([\eta]\phi_m)$ and $1/\gamma$ for KD and MCT, respectively.

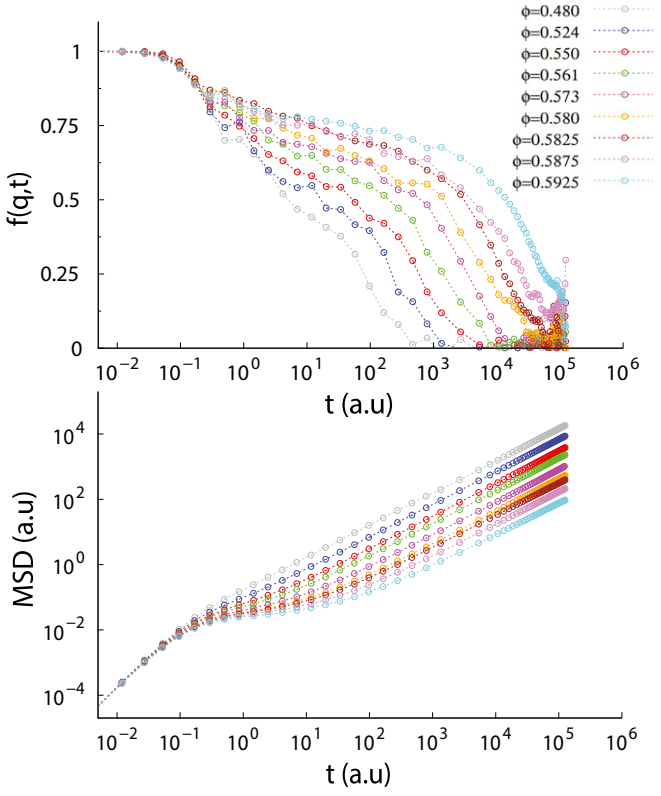

Fig. S4. (*Top*) Number-average intermediate scattering functions (ISF) from MD simulations for a range of volume fractions approaching the glass transition boundary, using polydispersity parameter $p = 0.20$ and scattering vector $q = 0.0366$ nm^{-1}, the smallest attempted here. (*Bottom*) Mean-square displacement (MSD) from event-driven molecular dynamics simulations as a function of time. Tangent slope at left shows delay time realm of ballistic motion in the event-driven MD simulations; tangent slopes at right show long-time diffusive realm.

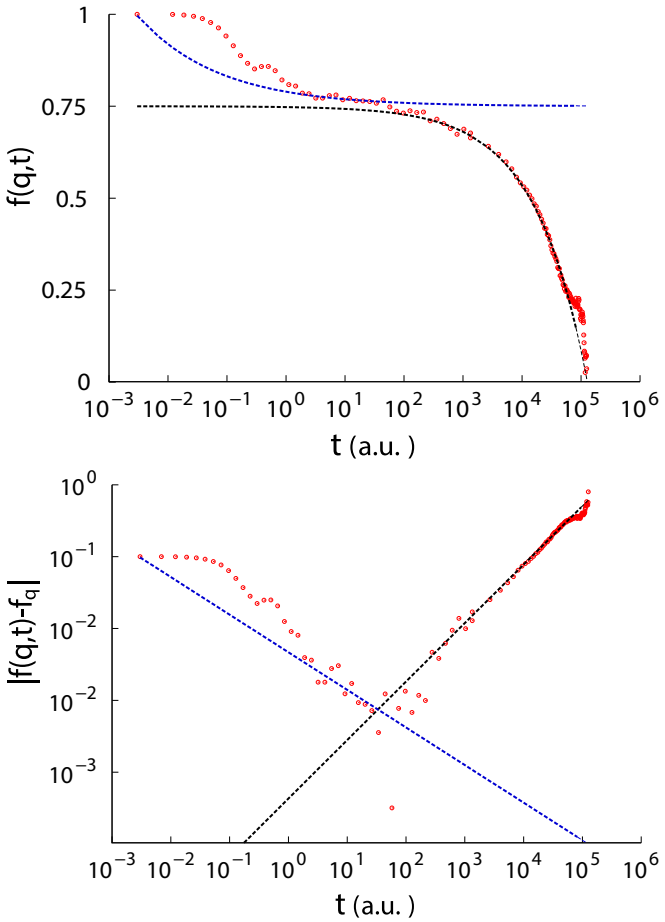

Fig. S5. (*Top*) ISF for $\phi = 0.5925$ from computer simulations. The fits are the MCT power laws. (*Bottom*) Rectification plot.

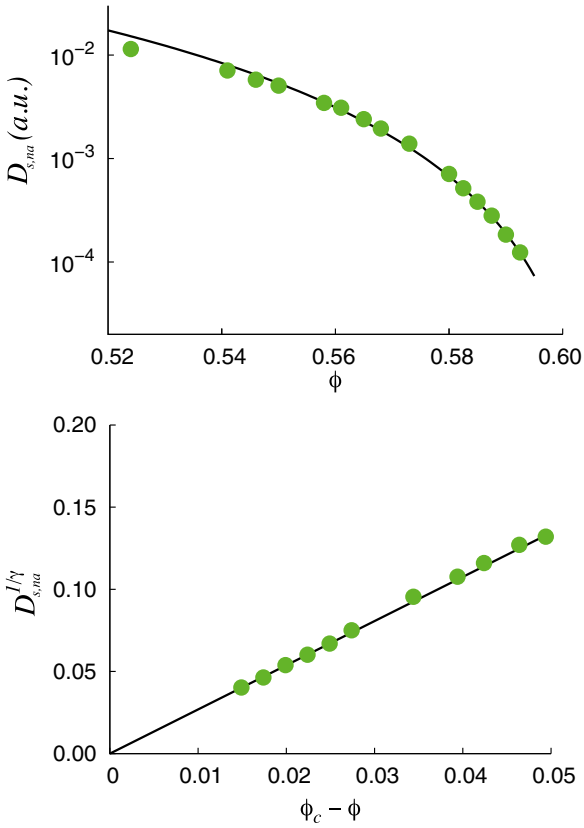

Fig. S6. (*Top*) Number-average self-diffusion coefficients $D_{s,\mathrm{na}}$ from MD simulations vs. volume fractions ϕ near ϕ_c. (*Bottom*) Replotted data from *Top*, showing power-law dependence of $D_{s,\mathrm{na}}$ on $\phi_c - \phi$ for $\phi_c = 0.6074$ and $\gamma = 2.8$.